Food Chemistry 407 (2023) 135173

Contents lists available at ScienceDirect

Food Chemistry

journal homepage: www.elsevier.com/locate/foodchem

New insights into the search of meat quality biomarkers assisted by Orbitrap Tribrid untargeted metabolite analysis and chemometrics

Borja Garlito [a,b], Miguel A. Sentandreu [c], Vicent Yusà [b], Mamen Oliván [d], Olga Pardo [e,f,*], Enrique Sentandreu [c,*]

[a] Enviromental and Public Health Analytical Chemistry, Research Institute for Pesticides and Water (IUPA), Universitat Jaume I, Av. Sos Baynat S/N, 12071 Castelló de la Plana, Spain
[b] Foundation for the Promotion of Health and Biomedical Research in the Valencian Region, FISABIO-Public Health, Av. Catalunya, 21, 46020 València, Spain
[c] Instituto de Agroquímica y Tecnología de Alimentos (IATA-CSIC), Calle Agustín Escardino, 7, 46980 Paterna, Valencia, Spain
[d] Servicio Regional de Investigación y Desarrollo Alimentario (SERIDA), Carretera de Oviedo, s/n, 33300 Villaviciosa, Asturias, Spain
[e] Public Health Laboratory of València, Av. Catalunya, 21, 46020 València, Spain
[f] Department of Analytical Chemistry, University of Valencia, Doctor Moliner 50, 46100 Burjassot, Spain

ARTICLE INFO

Keywords:
Untargeted metabolomics
Iterative LC-MS^n workflow
Meat quality biomarkers
Chemometric analysis
Acyl-carnitine intermediates
Validation assessment

ABSTRACT

Metabolite profiles of normal and defective dry, firm and dark (DFD) meat extracts with known ultimate pH (pHu) values were determined by Orbitrap Tribrid ID-X untargeted analysis coupled to chemometrics. An intelligent MS^3 AcquireX^{TM} workflow firstly approached the unambiguous characterization of detected features that were subsequently quantified by a complementary MS^1 study of biological replicates. Chemometric research revealed how threonylphenylalanine (overexpressed in normal meats) together to tetradecadienoyl- and hydroxydodecanoyl-carnitines (both overexpressed in DFD meats) appropriately grouped meat groups assayed. Robustness of such biomarkers was confirmed through a time-delayed study of a blind set of samples (unknown pHu) and evidenced limitations of pHu as an isolated parameter for accurate meat quality differentiation. Other acyl-carnitines also characterized DFD samples, suggesting interferences induced by pre-slaughter stress (PSS) on lipid catabolism that would explain accumulation of such intermediate metabolites. Results achieved can ease understanding of biochemical mechanisms underlying meat quality defects.

1. Introduction

After decades of evolution, cattle industry has been oriented towards the production of fat reduced and heavier finishing animals with improved carcass cutability for the sake of sustainable profitability (McNeill et al., 2012). This practice favors the breeding of oversized animals with increased susceptibility to stressing conditions (Fiems, 2012). This may explain the increasing occurrence of meat quality defects in the production chain such as dark, firm and dry (DFD) meats with undesirable color/flavor and reduced shelf-life, inflicting important economic losses for industry (Holdstock et al., 2014). Occurrence of DFD meats is related to depleted reservoirs of muscle glycogen previous to slaughter caused by the elevated glycogenolysis induced by pre-slaughter stress (PSS) motivated by intrinsic (i.e. sex, age, breed) and extrinsic (i.e. transportation, inadequate animal handling practices) factors (Ferguson & Warner, 2008). Such metabolic alterations preclude generation of lactic acid during conversion of muscle into meat, giving rise to abnormally high ultimate pH (pHu) values at the end of the maturation process. Easiness of pHu determination (normally at 24 h postmortem) made this measurement the standard operation protocol to determine the presence of DFD meats in the production chain. Nevertheless, there is no harmonized pHu criterion towards identification of DFD meats. According to the Meat Standards Australia (MSA) system, meats with pHu values higher than 5.7 can be considered as DFD (Loudon et al., 2018). In contrast, different studies establish such threshold beyond pH 6.0 considering the noticeable increasing of muscle water holding capacity (WHC) and the apparition of both a firm texture and off-flavors (Ponnampalam et al., 2017). Furthermore, there was argued how detection of DFD meat is not unfailingly related to high pHu values (Apaoblaza et al., 2020), thus increasing the need for more

* Corresponding authors at: Public Health Laboratory of València, Av. Catalunya, 21, 46020 València, Spain (O. Pardo); Instituto de Agroquímica y Tecnología de Alimentos (IATA-CSIC), C/ Agustín Escardino 7, 46980 Paterna, Valencia, Spain (E. Sentandreu).
E-mail addresses: pardo_olg@gva.es (O. Pardo), elcapi@iata.csic.es (E. Sentandreu).

https://doi.org/10.1016/j.foodchem.2022.135173
Received 27 September 2022; Received in revised form 5 December 2022; Accepted 6 December 2022
Available online 9 December 2022

accurate predictive approaches in meat quality assessment.

Recent studies highlighted how alterations on meat proteome induced by stress could be successfully addressed by the search of reliable biomarkers through proteomic strategies supported by liquid chromatography-mass spectrometry (LC-MS) analysis (Marco-Ramell et al., 2018). Despite of efficiency shown by traditional gel-based LC-MS approaches to unveil PSS protein biomarkers (Fuente-Garcia et al., 2019, 2020), analytical performance of modern LC-high resolution mass spectrometry (LC-HRMS) technology has recently allowed the development of straightforward gel-free proteomic pipelines for rapid biomarker hunting in meat quality evaluation (Sentandreu et al., 2021).

It must be emphasized how in current *trans*-omic era, combination of proteomic and metabolomic studies can provide a deeper biological understanding about the influence of PSS on meat quality, being also possible the integration of additional genetic (intrinsic) and environmental (extrinsic) factors (Kasper et al., 2020). Contrary to existing literature about the elucidation of protein/peptide biomarkers linked to meat quality affected by PSS, little is known about the search of reliable metabolite predictors for early detection of defective meat. Since the metabolome informs about the functional state of an organism and it is not commonly breed- or species-specific, metabolite research in PSS meat can have a great interest mainly for translational studies (Kasper et al., 2020). Metabolomic research of PSS was conducted in blood and meat mainly through exploratory nuclear magnetic resonance (NMR) approaches (Beauclercq et al., 2016; Cônsolo et al., 2021; Muroya et al., 2020) and, to a lesser extent, by targeted triple-quadrupole (QqQ) LC-MS analysis (Batchu et al., 2021). Inherent drawbacks of analytical platforms such as limited sensitivity (NMR) and flexibility (QqQ) can hinder efficiency in the search of reliable PSS metabolite biomarkers. Furthermore, there is a noticeable absence of metabolomic investigations assisted by modern LC-HRMS technology addressing the unveiling of unambiguous meat quality descriptors through untargeted approaches.

This study aimed to develop an effective metabolomic pipeline supported by state-of-the-art Orbitrap Tribrid analysis with intelligent data acquisition and chemometrics for the search of reliable PSS biomarkers. Normal and DFD (according to high pHu values) bovine meat samples were studied by qualitative Acquire X^{TM} iterative data dependent MS^3 (dd-MS^3) and quantitative full-MS^1 analyses coupled to chemometrics that conformed an innovative and efficient untargeted metabolomics strategy for data acquisition and interpretation. Efficiency of the methodology proposed was evaluated in terms of sensitivity, accuracy and robustness to provide reliable and unambiguous results to differentiate normal from defective meats. Analytical capacity provided by this alternative can favor the implementation of breakthrough LC-HRMS metabolite research for the creation of new insights into the understanding of responsible causes of the apparition of defective meats.

2. Materials and methods

2.1. Chemicals and reagents

LC-MS grade methanol (MeOH) and ultrapure water (H_2O) were from Merck KGaA (Darmstadt, Germany). Glacial acetic acid (HAc) was from Panreac (Barcelona, Spain). LC-MS grade formic acid (FA), ethanol (EtOH), ethylenediaminetetraacetic acid (EDTA, 99 % purity), Tris buffer (99 % purity) and 0.45 μm PVDF filters were from Scharlab (Scharlab S. L., Barcelona, Spain).

Stable isotopically labeled internal standard (SIL-IS) $^{13}C_6$-butylparaben was supplied by Cambridge Isotope Laboratories (CIL Inc., Andover, MA, USA), benzophenone-d_{10} was from Sigma Aldrich (St Louis, MO, USA) and AMMA-d_3 (*N*-acetyl-S-(2-carbamoylethyl)-l-cysteine-d_3) was from Toronto Research Chemicals (Toronto, Canada). All SIL-ISs had a minimum chemical and isotope purity of 95 %. A pooled SIL-IS mix solution was prepared in MeOH at a stock concentration of 0.25 μg·mL^{-1}, storing aliquots at −20 °C until use. Certified commercial standards (minimum purity of 95 %) terfenadine, Val-Tyr-Val, sulfaguanidine, sulfadimethoxine, reserpine, caffeine and acetaminophen were from Sigma Aldrich (St. Louis, MO, USA) for assurance/quality control (QA/QC) purposes. Individual QA/QC standard solutions (around 100 mg·L^{-1}) were prepared in acetone. A QA/QC mix solution containing all compounds at around 0.5 mg·L^{-1} was prepared by mixing all individual QA/QC solutions with acetone. Finally, a technical quality control standard solution (tQC) was prepared by mixing QA/QC standard and SIL-IS mix solutions in water:MeOH (80:20, v/v) (resultant working concentration of 0.01 and 0.07 μg·mL^{-1} for QA/QCs and SIL-ISs, respectively) which was aliquoted in 1 mL vials to avoid contamination and stored at −80 °C until use.

Pierce ™ FlexMix ™ solution from Thermo Fished Scientific (Rockford, IL, USA) was used for calibration of the LC-HRMS device in both positive and negative ionization modes before the injection of each analytical batch.

2.2. Sample preparation

A reference sample batch was made up by meat samples from 12 crossbred animals belonging to different breeds provided by a commercial abattoir in Asturias (Spain). Muscle samples were from *Longissimus thoracis et lumborum* (LTL) of yearling bulls slaughtered at 14–15 months of age according to EU regulations (Council Regulations (EC) No 853/2004 and No 1099/2009). Ten grams of LTL muscle were excised from the 13th rib at 24 h post-mortem and the epimysium was dissected. Meat aliquots were immediately vacuum-packed and stored at −80 °C until processed for metabolite extraction. Reference samples were classified (**Table S1A**) according to their pHu values as normal (n = 6, pHu ≤ 6.0) and DFD (n = 6, pHu > 6.0) replicates. Determination of pH was performed at the sixth rib of the LTL muscle at 24 h post-mortem.

A complementary blind (validation) batch (8 replicates, **Table S1B**) was prepared and analyzed with a 3-month delay than its reference counterpart. Blind replicates were from different individuals (from different breeds) than those considered in the reference set but shared the same geographical origin and manipulation procedure, keeping their pHu unknown until finishing their chemometric study.

Fig. S1 illustrates the sampling procedure followed to prepare the reference batch (**Table S1A**). Half a gram of LTL muscle sample was homogenized in 4 mL of extraction buffer (10 mM Tris pH 7.6 containing 0.25 M sucrose, 1 mM EDTA and 25 μL of protease inhibitor cocktail), centrifuged at 20,000 *g* for 20 min at 4 °C and the supernatant filtered through a 0.45 μm PVDF filter. Seventy microliters of each sample were mixed with 300 μL of chilled EtOH (containing 0.15 % FA), vortexed (20 s), stored at −20 °C for 30 min and centrifuged at 3600 *g* for 20 min at 4 °C. The pellet (proteins) was discarded and the supernatant was completely desiccated in a SPD121P SpeedVac vacuum concentrator (Thermo Scientific, San Jose, CA, USA). Samples were re-suspended in 80 μL of an aqueous 0.1 % FA solution and 30 μL of the SIL-IS stock solution (final sample volume and SIL-IS working concentration were 110 μL and 0.07 μg·mL^{-1}, respectively), vortexed, centrifuged at 20,000 *g* for 10 min and finally poured into LC-MS vials. Before isolated vial encapsulation of NORMAL and DFD replicates, aliquots of 20 μL from each sample were pooled (total volume of 240 μL) to conform the quality control sample (QC). Same sampling procedure was applied to the validation batch (**Table S1B**) to prepare the respective biological replicates. Reference and validation batches as well as, QC and tQC aliquots were stored at −80 °C until analyzed.

2.3. UHPLC-HRMS analysis of samples

A Thermo Vanquish Horizon UHPLC system (ThermoFisher Sci., San Jose, CA USA) was interfaced to a Thermo Orbitrap ID-X Tribrid mass spectrometer (ThermoFisher Sci., Bremen, Germany), with a heated electrospray interface (H-ESI) operating in separate positive and

negative ionization modes. An autocalibration source (EASY-IC) was embedded in the H-ESI probe to preserve mass accuracy during analyses according to infused lock masses (anions and cations from fluoranthene reagent). Metabolite separation was achieved in a Thermo Hypersil Gold, 150 × 2.1 mm, 1.9 μm particle size column (ThermoFisher Sci., San Jose, CA USA) using water and MeOH, both with HAc at 0.1 %, as mobile phase A and B, respectively, at a flow rate of 0.3 mL·min^{-1} under the following gradient conditions: initially 10 % B; linear 10–70 % B in 18 min; linear 70–98 % B in 3.5 min; held for 3.5 min for washing; 10 % B in 0.1 min and held for column equilibration for 5 min. The total running time was 30.1 min. The injection volume was 2 μL and autosampler and column temperatures were 8 °C and 35 °C, respectively.

Mass spectrometry conditions were: H-ESI voltage, 3.5 kV and 3.2 kV for positive and negative ionization modes, respectively; sheath gas, 60 arbitrary units (au); auxiliary gas, 20 au; ion transfer tube and vaporizer temperatures 290 °C and 330 °C, respectively. Samples from the reference batch (**Table S1A**) were separately analyzed through AcquireX^{TM} dd-MS^3 intelligent data acquisition and full-MS^1 approaches according to untargeted qualitative and quantitative purposes, respectively. Full-MS^1 analysis considered the 110–1100 *m/z* range at 120.000 FWHM (*m/z* 200) resolving power. MS^2 analysis was acquired by the Orbitrap analyzer at 15.000 FWHM (*m/z* 200) resolving power with a precursor *m/z* range of 110–1100 and the sequential MS^3 fragmentation was featured by the Linear Ion Trap (LIT). Further MS acquisition parameters are detailed in **Table S2**. Replicates belonging to the reference and validation batches were relatively quantified by full-MS^1 analysis.

2.4. TRIBRID ID-X acquisition workflow for untargeted metabolite determination of the reference batch

Fig. S2 summarizes the qualitative/quantitative data acquisition workflow considered in this study to ease understanding of the metabolomics pipeline proposed. Analyses were separately performed in positive and negative ionization modes. To enhance clarity of nomenclature used in this research, the term full-MS^1 refers to isolated (non-multiplexed) intact molecule quantitative experiments whereas MS^1 corresponds to parent ion assays embedded in multiplexed AcquireX^{TM} dd-MS^3 qualitative research.

Fig. S2A gives a general overview of the preliminary untargeted qualitative metabolite approach of the QC sample as suggested by Yusà et al. (2020) implementing the AcquireX^{TM} intelligent data acquisition technology (Thermo Fisher Scientific, San Jose, CA, USA) operating in Deep Scan (DS) mode for a detailed dd-MS^3 approach. Further AcquireX^{TM} operative details are provided by **Fig. S2**B indicating how a full-MS^1 analysis of blank (water/MeOH 90:10) and QC samples initially conformed the exclusion and inclusion mass lists, respectively. Briefly, two blank injections firstly conditioned the LC-HRMS system whereas the third blank conformed the exclusion (background) mass list. Then, one single MS^1 QC injection was performed to populate the raw inclusion mass list from which it was subtracted previous background masses giving rise to the definitive inclusion mass list. The exhaustive dd-MS^3 analysis of such targeted masses was achieved through three iterative injections of the QC sample. Features sampled for MS$^{n>1}$ analyses (whose MS^1 were initially listed in the definitive inclusion mass list) in a considered iteration were automatically moved from the definitive inclusion list to the dynamic exclusion list to avoid their analysis in subsequent iterations.

After AcquireX^{TM} DS dd-MS^3 acquisition, biological replicates of the reference batch were randomly analyzed in duplicate (n = 24) in both positive and negative full-MS^1 mode to ensure reliability of the untargeted quantitative study (Dudzik et al., 2018). A QC injection was intercalated throughout the sample list (total number of QC injections was 7). In addition, a tQC was also injected at the beginning and end of the reference sample list (n = 2). To test robustness of biomarkers initially proposed from the analysis of the reference sample set, same full-MS^1 quantitative approach was applied to the validation batch (**Table S1B**, n = 8) with a 3-month delay and considering same QC and tQC aliquots than before (total number of QC and tQC injections throughout the sample list was 3 and 2, respectively).

2.5. LC-HRMS data processing of quantitative full-MS^1 and qualitative Acquire X^{TM} DS dd-MS^3 approaches

Raw data files were automatically processed by Thermo Compound Discoverer™ v.3.2 (CD3.2 Thermo Fisher Scientific, San Jose, CA, USA). **Fig. S3** illustrates data analysis workflow followed in this study, finding instrumental settings fully detailed at the *supplementary file*. Briefly, this workflow performs peak picking, retention time alignment and peak grouping across all samples. Moreover it also predicts the elemental composition of all features extracted and enables interrogation of intact mass data (for both full-MS^1 and MS^1 regarding quantitative and qualitative assays, respectively) through in-house (embedded in CD3.2 related to intact mass data) and on-line repositories performing the similarity search of dd-MS^2 information (from AcquireX^{TM} assay) through mzCloud database (*https://www.mzcloud.org/*). Finally, QC-based batch normalization was applied through systematic error removal using random forest (SERRF) algorithm and the removal of the chemical background using blank samples.

Identification of unassigned metabolites by CD3.2 was externally carried out by MetFrag (https://ipb-halle.github.io/MetFrag/) *in silico* fragmentation tool with subsequent searches loading ChemSpider (*https://www.chemspider.com/*) and PubChem (*https://pubchem.ncbi.nlm.nih.gov/*) databases. In any case, mass tolerance for MS^1, MS^2 and MS^3 interrogations was set to 5 ppm, 10 ppm and 0.5 Da, respectively. Manual assessment of structural MS^3 information (from AcquireX^{TM} assay) was restricted to only those biomarkers conforming definitive discriminant models elucidated.

2.6. Statistical analysis

A multivariate analysis was performed on processed quantitative full-MS^1 data (integrated peak area) from the reference batch (**Table S1A**) aiming at finding discriminative features among meat groups assayed (normal *vs* DFD) using SIMCA 14.1 (Umetrics, Umea, Sweden) software. Resultant data matrices with the integrated peak area value of signals from peak picking extraction (in both positive and negative ionization modes) were log2 transformed and Pareto scaled. Thus, a preliminary principal component analysis (PCA) was done on raw full-MS^1 data to ensure the absence of outliers and to provide a general overview about sample replicates clusterization and QC positioning in the score plot. Features with a corrected relative standard deviation (RSD) higher than 20 % on peak area across the QCs were removed and subsequently checked to confirm the expected improvement in sample separation and QC positioning. A final PCA was calculated without QCs and considered the average value of sample replicates (analyzed in duplicate).

To highlight the most discriminant features (potential metabolite biomarkers) characterizing NORMAL and DFD samples, an orthogonal partial least square discriminant analysis (OPLS-DA) was conducted selecting signals with $|p[corr]| > 0.80$ (positive mode) and > 0.95 (negative mode) and with a variable influence on projection (VIP) higher than 1. Subsequently, univariate *t*-test analysis with Benjamini-Hochberg correction for false discovery rate (FDR) was performed and only those features with an adjusted p-value < 0.05 and a fold change between groups higher than 10 were finally selected (Benjamini & Hochberg, 1995).

Quality of models was evaluated by the goodness-of-fit test (R^2X), the proportion of the variance of the response variable that is explained by the model (R^2Y), the predictive ability parameter (Q^2) and significance of the model ($P_{CV\text{-}ANOVA}$). A 7-fold cross-validation (CV) and permutation tests on the responses (500 random permutations) were performed to test robustness and possible overfitting.

Performance of biomarkers originally proposed by the statistical analysis of the reference set (**Table S1A**) was lately (3-month delay) assessed through the validation batch (**Table S1B**) by checking the fit of the observations to the developed models. It must be emphasized that pHu of validation replicates was unknown at the time of their LC-HRMS and statistical analyses. This ensured the unbiased assessment of the discriminant competence of biomarkers proposed by the study of the reference batch.

2.7. Performance assessment of LC-HRMS analysis

LC-HRMS data quality assessment was conducted in full-MS^1 at 120.000 FWHM resolving power (m/z 200) in positive and negative ionization modes according to the following considerations:

- System contamination was evaluated through the injection of the mobile phase at initial chromatographic conditions (water/MeOH 90:10 with HAc 0.1 %) to detect the presence of polysyloxanes (PSX) and poly(ethylene glycol) (PEG) interfering species. Contamination was checked before the analysis of reference and validation batches. Limit of presence was defined by the mean ± 3·SD standard deviation (SD) of registered data from our internal Shewhart chart.
- A suitability test was carried out before analysis of reference and validation batches in both polarity ionization modes. Performance of the LC-HRMS device was qualified regarding stability of retention time (Rt), signal intensity (integrated full-MS^1 peak area) and mass accuracy on QA/QC standards according to data and limits (<mean ± 3·SD) from our internal Shewhart chart.
- Signal drift of the LC-HRMS system by time was assessed according to full-MS^1 response of analytes populating the tQC sample injected at the beginning and end of the reference and validation sample lists. Results were expressed as the integrated peak area ratio of each isolated standard at end/initial sequence time. There was assumed a maximum signal variation of 30 % for each standard as an acceptable quality threshold.
- Run-to-run full-MS^1 chromatographic performance, mass accuracy and signal variability were also evaluated in positive and negative ionization modes for SIL-ISs in QC sample interleaved throughout reference and validation sample lists. A maximum Rt shift of ± 0.2 min and a maximum peak width at FWHM of 0.1 min for individual SIL-IS were established as valid constraints for proper data acquisition. Full-MS^1 mass accuracy was thresholded at 5 ppm and a maximum signal variability of 30 % expressed in terms of relative standard deviation (RSD) from each individual SIL-IS integrated peak area were used as acceptability constraints.

3. Results and discussion

Experimental LC-HRMS data in mzML format is freely available at https://saco.csic.es/index.php/s/BYGGteeCFAjypXo.

3.1. Performance assessment of the LC-HRMS platform of analysis

Before data processing of reference and validation batches, a suitability analysis was carried out to certify proper instrumental performance for the achievement of reliable results. The system contamination test indicated a normal presence (<mean ± 3·SD) of PSX and PEG species before running reference and validation sample lists. Overall, results from the suitability test were between the acceptance limits (**Fig. S4**A). Signal drift associated to heavy-duty LC-HRMS operation was below 30 % without drop decay evidences in the response of QA/QC standards from tQC sample after completing the analysis of the reference (blue triangles) and validation (orange squares) sample lists (**Fig. S4**B). Finally, run-to-run control (**Fig. S4**C) certified the high instrumental performance achieved in this study showing a maximum Rt shift of 0.03 min, a maximum mass error of 4.1 ppm and peak area integration RSDs below 12 % regarding SIL-ISs from QCs injected throughout the reference (blue triangles) and validation (orange squares) sample lists.

3.2. Qualitative untargeted AcquireX^{TM} metabolite analysis of the reference batch

Fig. S5 shows the updated number of features populating the inclusion and exclusion lists across iterations performed by the AcquireX^{TM} dd-MS^3 workflow analysis proposed (**Fig. S2**, described in section 2.4.) regarding QC sample analyzed in positive and negative ionization modes. Total number of MS^1 features achieved after the 3-iteration duty cycle was about 47,000 and 19,000 in ESI^+ and ESI^-, respectively, obtaining MS^3 structural information of 33,278 (ESI^+) and 7647 (ESI^-) among them. After this preliminary qualitative screening, the search of efficient meat quality descriptors was approached through the chemometric analysis of full-MS^1 data from the quantitative study of the reference batch (untargeted quantitative fingerprinting, see below) but just considering those aforementioned features with available MS^3 information (coarse discriminant candidates). Thus, unambiguous identification of full-MS^1 features with clear discriminant capabilities proposed by the chemometric (quantitative) approach was further refined by AcquireX^{TM} DS dd-MS^3 qualitative results.

3.3. Untargeted quantitative fingerprinting of the reference batch: Multivariate analysis

A PCA analysis of the full-MS^1 data of coarse discriminant candidates was constructed with the reference set to check instrumental reproducibility (**Fig. S6A**). Then, data from biological replicates (n = 12) and QCs (n = 4) was filtered by choosing only those features (filtered coarse discriminant candidates) with a corrected RSD lower than 20 % on peak area across the QCs which were also present in at least 60 % of QC injections (giving rise to 32,444 and 7475 features in ESI^+ and ESI^-, respectively, **Fig. S6B**). There was obtained a similar clusterization than that exhibited by **Fig. S6A** with a tight positioning of QCs, certifying run-to-run reproducibility of the whole analyte fingerprint of samples assayed in the same line than shown by SIL-ISs in the preliminary instrumental performance assessment (Fig. S4C). A final PCA of was calculated without QC replicates and considering the average value of sample duplicates according to ionization modes assayed (averaged PCA models). Averaged models (Fig. 1) successfully differentiated, mainly in negative mode, NORMAL and DFD meat groups describing the first two PC components around 49 % and 53 % of variance in ESI^+ and ESI^- models, respectively.

Supervised OPLS-DA models were developed from the averaged PCA data to maximize differences between meat groups assayed. Most discriminant features were highlighted according to the S-Plot in which signals located far out on the wings of the S combined high model influence with high reliability (see Fig. 2A and 2B). As a result, 37 and 5 features (encircled data points in Fig. 2A and 2B) with $|p(corr)| > 0.8$ (>0.95 in ESI^-), VIP > 1, adjusted p-value < 0.05 and fold change > 10 were selected in ESI^+ and ESI^-, respectively, to generate reliable predictive models (see Fig. 2C and 2D) whose statistical discriminant capabilities are summarized in **Table S3** and fully characterized in Table 1. As we can see, even with acceptable R^2X and R^2Y values, a poor predictive capacity was achieved by ESI^+ model (37 features) with a very low Q^2, clearly suggesting a possible model overfitting. In contrast, three efficient predictive models were developed in ESI^- based on two (model A), three (model B) and five (model C) features exhibiting excellent discriminant attributes (**Table S3**) that provided a remarkable differentiation between meat groups assayed. From this, features populating ESI^- discriminant models achieved the status of potential meat biomarkers, using such nomenclature from now on throughout the discussion section.

To test robustness and the absence of possible overfitting of ESI^+ and ESI^- predictive models (**Table S3**), 7-fold cross-validation and

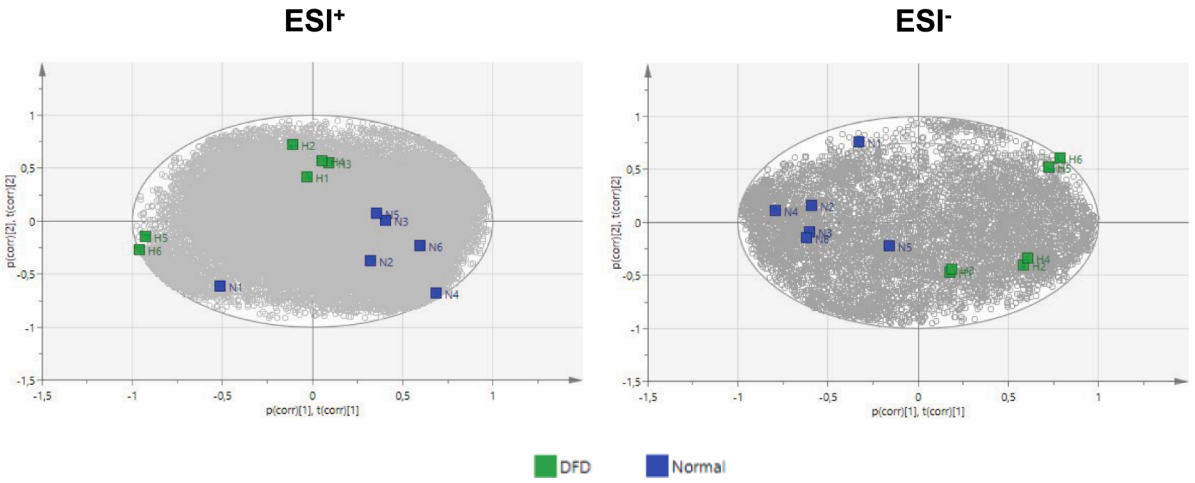

Fig. 1. Averaged PCA biplot (loadings *vs* features, samples analyzed in duplicate) from ESI^+ (left) and ESI^- (right) quantitative full-MS^1 analysis of the reference batch. Variance described by the first two PC components was around 49 % and 53 % in ESI^+ and ESI^- models, respectively.

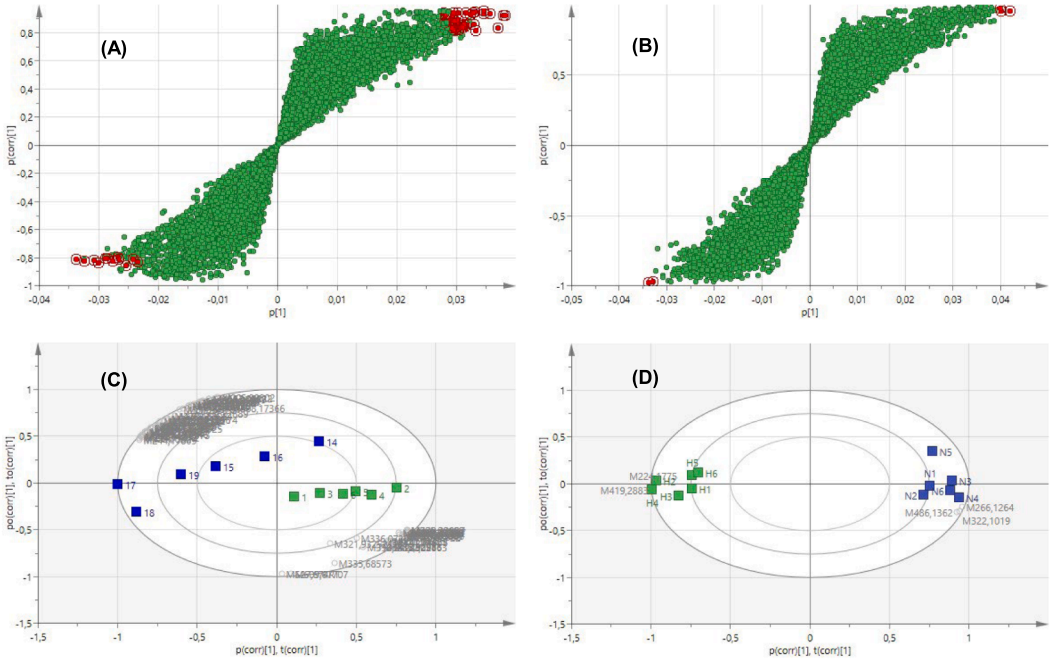

Fig. 2. S-plot obtained from the A) ESI^+ and B) ESI^- supervised OPLS-DA models from the averaged PCA data achieved by the quantitative multivariate analysis of the reference batch. Encircled red dots correspond to discriminant features accomplishing $|p(corr)| > 0.8$ (>0.95 in ESI-), VIP > 1, adjusted p-value < 0.05 and fold change > 10. OPLS-DA biplot (loadings *vs* features) of individuals and the C) 37 discriminant features from ESI^+ and D) 5 from ESI^-.

permutation tests on their responses (500 random permutations) were performed. Fig. S7 depicts the combined scatter plot of cross-validated (CV) and regular score vectors of the OPLS-DA discriminant models. It must be highlighted that the scatter plot of CV score vectors (orange dots) is analogous to the scatter plot of regular score vectors (blue dots) but indicated how sensitive was the discriminant model considering the iterative exclusion of an observation in the reference batch. Small differences between CV and regular score vectors meant a high model stability as shown by A (2 biomarkers) and B (3 biomarkers) ESI^- models (**Figs. S7A and S7B**, respectively) perfectly clustering NORMAL (blue circle clustering) and DFD (green circle clustering) replicates. In contrast, ESI^- C and ESI^+ predictive alternatives (**Figs. S7C and S7D,** respectively) had a noticeable spreading of sample groups. Thus, only A and B ESI^- discriminant models (Table S3) were considered for external validation through the study of the blind (validation) batch.

3.4. External validation of predictive A and B ESI^- discriminant models

External validation also aimed at the consideration of biological and instrumental variabilities as a source of error for discriminant models that could lead to misclassification of samples out of those belonging to the reference batch. Deviations in peak area integration were counteracted by SERRF normalization based on quality control (QC) correction. Briefly, SERRF works with a Random Forest machine learning algorithm (Breiman, 2001) which uses QC samples injected throughout reference and validation sample lists to build a model that estimates the systematical error (batch effect, day-to-day/run-to-run LC-HRMS signal variation, etc.) that is subsequently considered for signal normalization (Fan et al., 2019). Fig. S8 shows PCA of the averaged raw (A) and SERRF normalized (B) quantitative full-MS^1 data from filtered coarse discriminant candidates (see section 3.3.) in reference and validation batches

Table 1
Main discriminant features highlighted by the S-Plot representation of OPLS-DA models (**Fig. S7**) from the study of the reference sample batch.

#Compound	Tentative Identification[a]	Theoretical Formula	Theoretical MW[b]	ΔMass (ppm)[c]	RT (min)	Ionization mode	Adj p-value	Fold change[d]	Predictive model[e]
1	N/F	$C_{15}H_{27}N_4O_{12}P$	486,1362	−0,22	1,14	(-)	0.0008	130	ESI^- C
2	3,5-dihydroxyphenyl-dihydrogenphosphate	$C_6H_7O_6P$	205,99802	0	1,27	(+)	0,03	10	ESI^+
3	D-myo-inositol-1,2-cyclicphosphate	$C_6H_{11}O_8P$	242,01917	0,07	1,27	(+)	0,02	16	ESI^+
4	**N/F**	**$C_{21}H_{35}N_3O_{16}$**	**585,20187**	**0,24**	**1,29**	**(+)**	**0,005**	**12**	ESI^+
5	N/F	$C_{19}H_{27}N_6O_9P_3S$	608,07689	−0,68	1,32	(+)	0,03	26	ESI^+
6	L-asparagine	$C_4H_8N_2O_3$	132,05348	−0,11	1,54	(+)	0,0001	44	ESI^+
7	L-tyrosine	$C_9H_{11}NO_3$	181,07385	−0,23	1,85	(+)	0,007	71	ESI^+
8	ala-tyr	$C_{12}H_{16}N_2O_4$	252,11103	0,08	1,85	(+)	0,004	56	ESI^+
9	arg-leu	$C_{12}H_{25}N_5O_3$	287,19576	0,09	2,59	(+)	0,02	23	ESI^+
10	N/F	$C_{15}H_{18}N_4O_5$	334,12774	0,06	2,67	(+)	0,007	14	ESI^+
11	ala-leu-gly	$C_{11}H_{21}N_3O_4$	259,15327	0,23	2,93	(+)	0,004	41	ESI^+
12	phe-ala	$C_{12}H_{16}N_2O_3$	236,1161	0,05	2,95	(+)	0,01	29	ESI^+
13	thr-leu	$C_{10}H_{20}N_2O_4$	232,14232	0,05	3,12	(+)	0,01	35	ESI^+
14	met-tyr	$C_{14}H_{20}N_2O_4S$	312,11443	0,17	3,19	(+)	0,03	34	ESI^+
15	N/F	$C_8H_{12}N_2O_4S$	232,05183	0,24	3,62	(+)	0,004	52	ESI^+
16	N/F	$C_8H_{10}N_2O_3S$	214,04125	0,17	3,62	(+)	0,004	16	ESI^+
17	asp-val-lys	$C_{15}H_{28}N_4O_6$	360,20109	0,57	3,70	(+)	0,002	32	ESI^+
18	thr-phe	$C_{13}H_{18}N_2O_4$	266,1264	−0,98	3,93	(-)	0.02	54	ESI^- A, B, C
	thr-phe	$C_{13}H_{18}N_2O_4$	266,12668	0,1	3,97	(+)	0,04	73	ESI^+
19	ile-tyr	$C_{15}H_{22}N_2O_4$	294,15802	0,23	4,01	(+)	0,02	33	ESI^+
20	phe-val	$C_{14}H_{20}N_2O_3$	264,14743	0,15	4,77	(+)	0,003	27	ESI^+
21	leu-ile	$C_{12}H_{24}N_2O_3$	244,17874	0,17	5,16	(+)	0,0001	26	ESI^+
22	leu-tyr	$C_{15}H_{22}N_2O_4$	294,15804	0,28	5,18	(+)	0,0002	35	ESI^+
23	met-leu	$C_{11}H_{22}N_2O_3S$	262,13513	0,05	5,32	(+)	0,01	16	ESI^+
24	val-phe	$C_{14}H_{20}N_2O_3$	264,14743	0,13	5,64	(+)	0,007	24	ESI^+
25	ile-ile-lys	$C_{18}H_{36}N_4O_4$	372,27381	0,42	5,65	(+)	0,003	37	ESI^+
26	leu-leu	$C_{12}H_{24}N_2O_3$	244,17874	0,18	6,84	(+)	0,002	22	ESI^+
27	leu-phe	$C_{15}H_{22}N_2O_3$	278,16309	0,16	6,99	(+)	0,0008	18	ESI^+
28	leu-gly-phe	$C_{17}H_{25}N_3O_4$	335,18452	0,05	7,55	(+)	0,0006	31	ESI^+
29	N/F	$C_{12}H_{22}N_2O_4S_2$	322,10199	−0,33	7,66	(-)	0.03	60	ESI^- C
30	phe-leu	$C_{15}H_{22}N_2O_3$	278,16307	0,08	8,19	(+)	0,006	25	ESI^+
31	**hydroxydodecanoylcarnitine adduct (+OAc)**	**$C_{21}H_{41}NO_7$**	**419,28831**	**0,02**	**18,02**	**(-)**	**0.00002**	**23**	ESI^- B, C
	hydroxydodecanoylcarnitine	**$C_{19}H_{37}NO_5$**	**359,26729**	**0,33**	**18,04**	**(+)**	**0,0004**	**20**	ESI^+
32	**tetradecadienoic acid**	**$C_{14}H_{24}O_2$**	**224,17751**	**−0,52**	**19,76**	**(-)**	**0.001**	**54**	ESI^- A, B, C
	tetradecadienoylcarnitine	**$C_{21}H_{37}NO_4$**	**367,27241**	**0,41**	**19,77**	**(+)**	**0,007**	**71**	ESI^+
33	**hydroxyhexadecadienoylcarnitine**	**$C_{23}H_{45}NO_5$**	**411,2986**	**−1,37**	**20,18**	**(+)**	**0,007**	**19**	ESI^+
34	**hydroxytetradecanoylcarnitine**	**$C_{21}H_{41}NO_5$**	**387,29864**	**0,43**	**20,41**	**(+)**	**0,0005**	**26**	ESI^+
35	**hydroxyhexadecenoylcarnitine**	**$C_{23}H_{43}NO_5$**	**413,31432**	**0,47**	**20,78**	**(+)**	**0,002**	**10**	ESI^+
36	**hexadecadienoylcarnitine**	**$C_{23}H_{41}NO_4$**	**395,3037**	**0,35**	**20,94**	**(+)**	**0,04**	**125**	ESI^+
37	**hydroxyoctadecadienoylcarnitine**	**$C_{25}H_{45}NO_5$**	**439,32989**	**−1,3**	**21,22**	**(+)**	**0,02**	**17**	ESI^+
38	**hydroxyhexadecanoylcarnitine**	**$C_{23}H_{45}NO_5$**	**415,32987**	**0,24**	**21,34**	**(+)**	**0,02**	**25**	ESI^+
39	**hydroxyoctadecenoylcarnitine**	**$C_{25}H_{47}NO_5$**	**441,34556**	**0,32**	**21,53**	**(+)**	**0,006**	**33**	ESI^+

[a] Tentative assignments from automated Compound Discoverer analysis of MS^1 and MS^2 data from AcquireX™ assay (see section 2.5). Light and bold typeface are referred to assignments exhibiting a higher abundance in NORMAL and DFD meat groups assayed, respectively.
[b] Theoretical neutral mass.
[c] Mass shift considering theoretical and observed masses.
[d] Fold-change calculated as the ratio (higher/lower) of averaged values across replicates of each feature in NORMAL and DFD meat groups assayed.
[e] Statistical discriminant capabilities of ESI^+ and ESI^- models from OPLS-DA analysis are detailed in Table S3. N/F: match not found.

analyzed with a 3-month delay. As **Fig. S8B** evidenced, SERRF normalized QC samples (red dots) embedded in both batches assayed (same QC distributed throughout the reference and validation sample lists giving rise to a total number of 7) were all tightly clustered, demonstrating the high quality data acquisition and the proper batch-to-batch data correction performed in this research through SERRF normalization.

Accuracy of biomarkers belonging to A and B models (detailed in Table 1) was utterly assessed by their application to appropriately classify (NORMAL or DFD) samples populating the validation batch. As shown in Fig. 3, both models (A, 2 biomarkers and B, 3 biomarkers) gave rise to an acceptable classification of all blind replicates with the exception of VB1 sample by model B. However, model A predicted VB5 and VB6 samples outside Hotelling's T2 ellipse (0.05 significance) limits on y-axis (Fig. 3A), which could be related to the limited number of samples in the training (reference) set that was not representative enough (n = 12). Furthermore, model B plotted all validation (blind) samples between the Hotelling's T2 ellipse (0.05 significance), which could be explained by better description of within class variability by considering three biomarkers (instead those two from A model).

According to the traditional classification of meat restricted to only pHu measurement, number of correct NORMAL/DFD assignments reached by A and B models applied to the validation batch were 7 over 8, in both cases. Very interestingly, this apparently "isolated mismatch" (VB8 with pHu 6.15, **Table S1B**) was classified as NORMAL by both discriminant models (Fig. 3). This result can be explained according to previous studies stating how classification of defective meats (normal *vs* DFD) cannot be entirely addressed just considering pHu values (Fuente-García et al., 2021; Sentandreu et al., 2021). This is of special relevance in those cases neighboring the pH 6.0 boundary (i. e. VB 1 and 8, **Table S1B**), making feasible the apparition of meats with pHus above 6.0 exhibiting a normal behavior and *vice versa*. Similarly, VB1 replicate (pHu 5.83) also deserved special attention since its theoretical classification ruled by only pHu matched the statistical verdict suggested by both discriminant models but it was predicted close to the DFD limit (mainly in the case of model B, Fig. 3B), making evident uncertainties

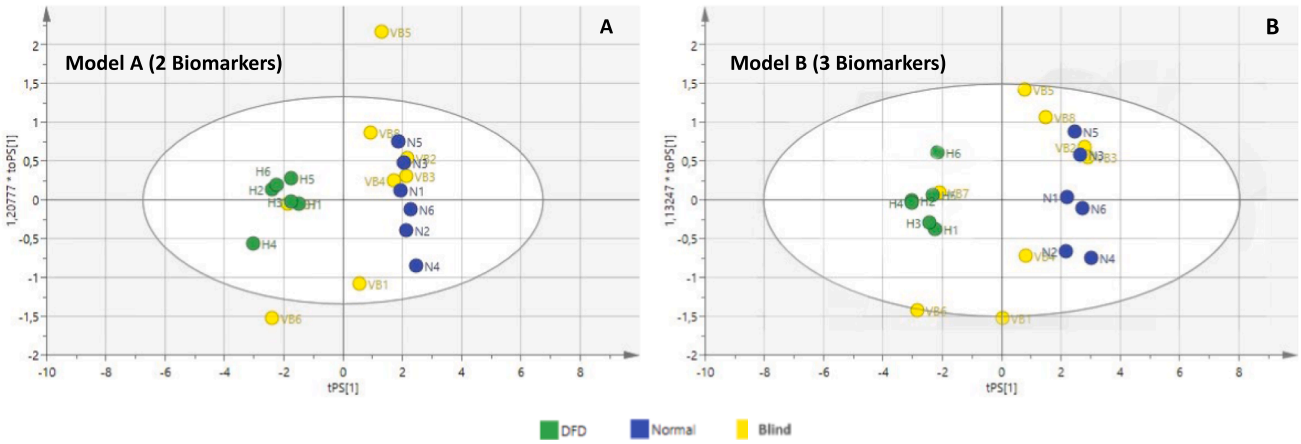

Fig. 3. Validation of ESI⁻ OPLS-DA discriminant models proposed (A, two biomarkers; B, three biomarkers) through the combined scatter plot of reference and validation batches considering Hotelling's T2 ellipse with a 0.05 significance. Colors used: NORMAL (blue dots), DFD (green dots) and BLIND (yellow dots).

about correct classification of meats with pHus around 6.0.

3.5. *Validation of tentative identification of metabolite biomarkers made by Acquire X^{TM} DS dd-MS^3 analysis*

Metabolomic studies in food certification are mainly discriminative and predictive, but appropriate identification of biomarkers is essential to understand sample classification (Righetti et al., 2018). In this research, there was finally proposed 3 statistically significant ESI⁻ biomarkers from initial 39 ESI$^+$/ESI⁻ candidates (see Table 1), all tentatively identified by automated CD3.2 analysis of MS^1-MS^2 data according to the five-level identification scale developed by Schymanski et al (2014). Tetradecadienoylcarnitine (models A and B), hydroxydodecanoylcarnitine (model B) and threonylphenylalanine (Thr-Phe, models A and B) were level 3 identified since their unequivocal molecular formula was unambiguously assigned by CD3.2 to biomarker candidates according to MS^1 mass accuracy (5 ppm mass deviation) combined with their respective ESI$^+$/ESI⁻ dd-MS^2 spectra. However, such spectral information was not enough to differentiate possible positional isomers of suggested descriptors. Thus, a manual inspection of their dd-MS$^{1\text{-}3}$ information was performed to refine their structural properties.

As an example, Fig. 4 depicts ESI$^{+/-}$ extracted ion chromatograms and MS^2 spectra of tetradecadienoylcarnitine. The [M−H]⁻ of tetradecadienoic acid (mass error of 0.5 ppm) was detected in ESI⁻ (in source fragment from the loss of the carnitine residue occurred in negative ionization, Fig. 4A) as well as its characteristic, but not specific, MS^2 product ion (Fig. 4B) at *m/z*⁻ 59.01346 (mass error of 6.6 ppm) considering three stepped HCD fragmentation energies. At the same retention time than tetradecadienoic acid, there was also present an ion

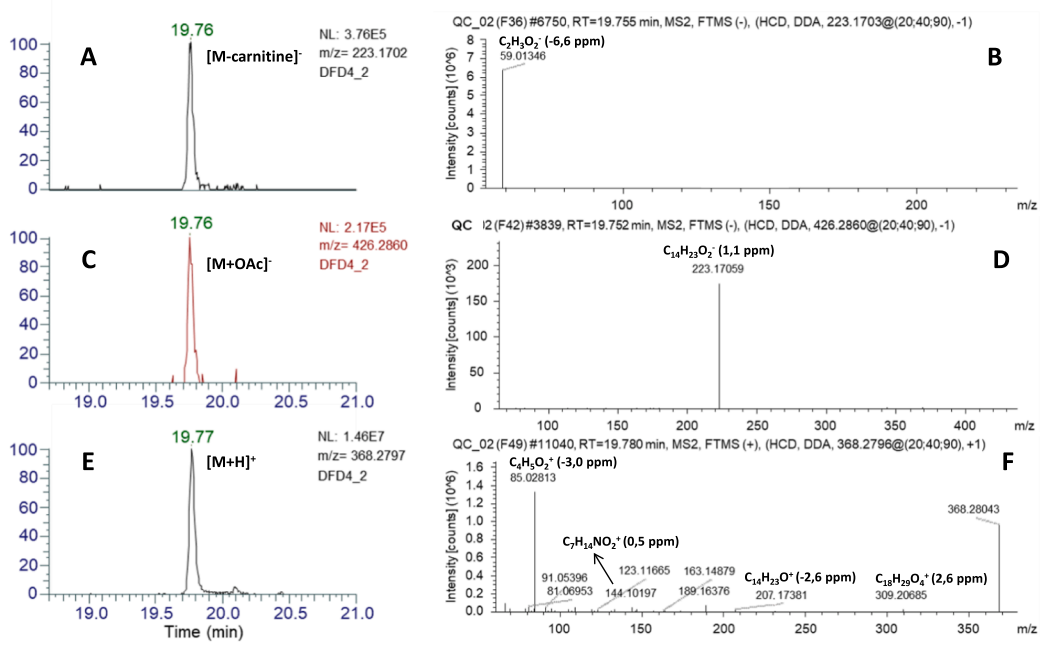

Fig. 4. Dd-ms^2 spectral information of tetradecadienoylcarnitine from QC sample provided by Acquire X^{TM} analysis (further details in Table S4). A, extracted ion chromatogram (XIC) of [M−H]⁻ corresponding to tetradecadienoic acid; B, MS^2 ESI⁻ spectra of tetradecadienoic acid; C, XIC of [M + OAc]⁻ from tetradecadienoylcarnitine; D, MS^2 ESI⁻ spectra of the tetradecadienoylcarnitine acetate adduct; E, XIC of [M + H]$^+$ from tetradecadienoylcarnitine; F; MS^2 ESI$^+$ fragmentation pattern of tetradecadienoylcarnitine.

at m/z^- 426.2860 (Fig. 4C) whose 203.1158 mass increase could correspond to an acetate adduct of carnitine (mass error of 0.3 ppm) from the incorporation of acetic acid into the mobile phase. The presence of such adduct (acylcarnitine-tetradecadienoid acid) was feasible since acylcarnitine compounds have an amphoteric character whose quaternary amine charge can be neutralized by acetate ions from the mobile phase. This hypothesis was supported by MS^2 analysis of precursor ion at m/z^- 426.2860 (Fig. 4D) giving rise to the apparition of the product at m/z^- 223.1706 (mass error of 1.1 ppm) corresponding to tetradecadienoic acid after the loss of the acylcarnitine moiety (as shown by Fig. 4A). Due to the amphoteric character of tetradecadienoylcarnitine and to proper ensure its unambiguous characterization, ESI^+ data was also checked. The $[M + H]^+$ of tetradecadienoylcarnitine (m/z^+ at 368.2797, mass error of 0.41 ppm) was appropriately aligned to its aforementioned negatively charged counterparts (Fig. 4E). Its MS^2 breakdown pattern (Fig. 4F) revealed the presence of fragments at m/z^+ 85.0281, 309.2069, 207.1738, 189.1638, 144.1020 and 91.0540 (mass shifts below 3 ppm in all cases) that were fully compatible to the tetradecadienoylcarnitine structure (**Table S4**).

The structural characterization procedure all three biomarkers proposed was moved forward to MS^3 assay, summarizing **Table S4** main findings from the manual inspection of their MS^{1-3} data provided by AcquireX^{TM} DS dd-MS^3 analysis. It must be emphasized how tentative assignments proposed by CD3.2 dd-MS^2 data processing (Table 1) were comparable to those manually elucidated (**Table S4**), confirming reliability of automated qualitative analysis performed.

3.6. *Biological significance of elucidated meat quality biomarkers*

Results obtained in this research revealed significant increased levels of long chain acyl-carnitines (Table 1) with special statistical relevance of tetradecadienoylcarnitine and hydroxydodecanoylcarnitine in DFD meats compared to normal meats. Such compounds are metabolic intermediates of lipid catabolism whose main role is the transport of acyl

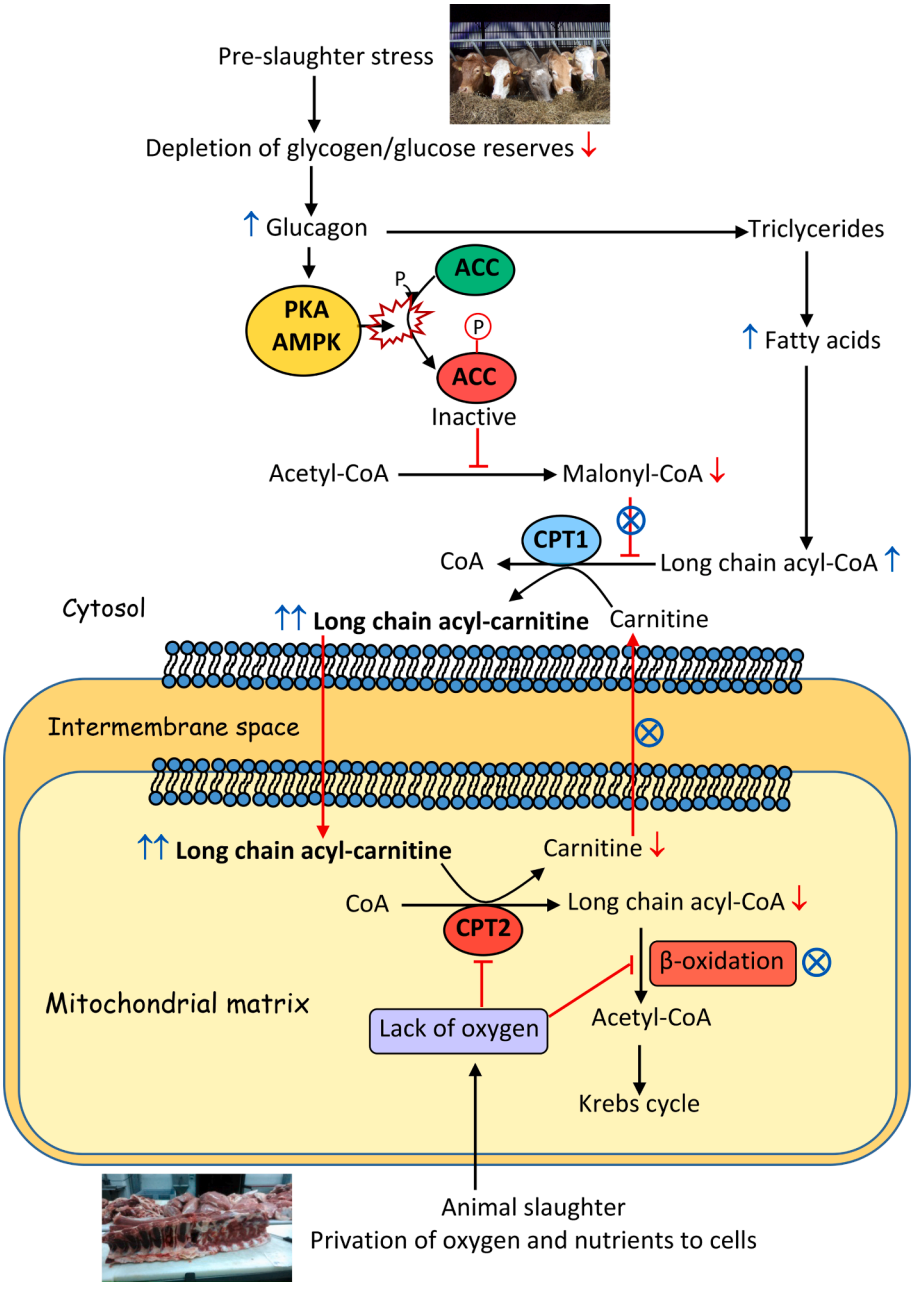

Fig. 5. Overview of the dysfunctional metabolism of long chain acyl-carnitines occurring in muscle cells of pre-slaughter stressed animals.

groups from the cell cytosol into the mitochondrial matrix, so that they can enter into the β-oxidation to be broken down to produce energy. Their increase in DFD meats would be directly related to the particular muscular cell dysfunctional situation occurring in pre-slaughter stressed animals as depicted by Fig. 5, finding how affected individuals are characterized by a depletion of their glycogen/glucose reserves prior to slaughter (Fuente-García et al., 2022). Consequently, glucagon will be released which, in turn, will activate cAMP-dependent protein kinase (PKA), inactivating acetyl-CoA carboxylase (ACC) through phosphorylation (Fig. 5). The increase of AMP/ATP ratio will also allow that AMP-activated protein kinase (AMPK) phosphorylates and inactivates ACC, thus inhibiting the malonyl-CoA synthesis. This will open the door to fatty acid catabolism since activity of carnitine acyl-transferase 1 (CPT1) is no longer inhibited by malonyl-CoA. It must be emphasized how CPT1 enables the conversion of long-chain acyl-CoA into long-chain acyl-carnitines, making their transport feasible from the cell cytosol into the mitochondrial matrix via acyl-carnitine/carnitine transporter (Nelson & Cox, 2017). In the matrix, the acyl group is transferred again to mitochondrial CoA, releasing carnitine to return to the outer mitochondrial membrane (Makrecka et al., 2014). PSS conditions hinders the oxygen supply and promotes a situation of cellular stress in muscle that can interrupt the mitochondrial oxidative metabolism and ATP production through the Krebs cycle. Failure of mitochondrial respiration will inactivate activity of carnitine acyltransferase 2 (CPT2) in cell matrix, blocking the conversion of long-chain acylcarnitines to long-chain acyl-Coa whose entrance into β-oxidation pathway would be impaired (Dambrova et al., 2021). Final consequence of PSS would be the accumulation of metabolic intermediates such as long chain acyl-carnitines (Fig. 5) as evidenced in DFD samples assayed (Table 1).

Regarding multiple etiology of the third metabolite biomarker elucidated in this research (threonylphenylalanine), further research is needed to refine our knowledge about biochemical reasons of its under-expression in DFD meats studied. In any case, usefulness of such dipeptide as a meat quality descriptor was appropriately addressed considering results achieved.

4. Conclusions

The untargeted metabolomics workflow proposed successfully addressed discrimination of normal and DFD beef samples assayed through the unveiling of three robust biomarkers. The analysis of a validation (blind) batch of samples further confirmed reliability of tetradecadienoylcarnitine, hydroxydodecanoylcarnitine and threonylphenylalanine as unambiguous meat quality descriptors, highlighting risks associated with the only consideration of pHu as the only parameter to detect the presence of true DFD meats (mainly in those cases with pHu close to 6). Interestingly, outside tetradecadienoylcarnitine and hydroxydodecanoylcarnitine there were also other long chain acyl-carnitines species overexpressed in DFD meats, suggesting how accumulation of such metabolite intermediates can be the result of the increase induced by PSS on lipid catabolism.

Future metabolomic investigations considering different bovine breeds are needed in the search of reliable meat quality biomarkers that have to be unambiguously characterized by rigorous analytical standards. Results demonstrated that untargeted metabolomic research supported by innovative LC-HRMS strategies in conjunction with chemometrics, is a powerful tool for accurate beef classification far beyond the easy-to-do but inaccurate pH determinations. Moreover, methodology proposed can facilitate the understanding of biochemical pathways involved in the apparition of defective meats.

CRediT authorship contribution statement

Borja Garlito: Data curation, Formal analysis, Investigation, Methodology, Software, Validation, Visualization, Writing – original draft, Writing – review & editing. **Miguel A. Sentandreu:** Conceptualization, Formal analysis, Investigation, Methodology, Funding acquisition, Project administration, Resources, Visualization, Writing – original draft, Writing – review & editing. **Vicent Yusà:** Formal analysis, Investigation, Methodology, Funding acquisition, Project administration, Resources, Writing – original draft, Writing – review & editing. **Mamen Oliván:** Investigation, Methodology, Funding acquisition, Resources. **Olga Pardo:** Investigation, Methodology, Supervision, Visualization, Resources, Writing – original draft, Writing – review & editing. **Enrique Sentandreu:** Conceptualization, Data curation, Formal analysis, Investigation, Methodology, Supervision, Validation, Visualization, Writing – original draft, Writing – review & editing.

Declaration of Competing Interest

The authors declare that they have no known competing financial interests or personal relationships that could have appeared to influence the work reported in this paper.

Acknowledgments

Borja Garlito thanks Spanish Ministerio de Universidades for his Margarita Salas postdoctoral grant (MGS/2021/25 (UP2021-021)) financed by the European Union-NextGenerationEU. Authors acknowledge the European Commission for the financial support received through the European Regional Development Funds (ERDF) Operational Programme of the Valencia Region (2014-2020). Authors are also indebted to RTI2018-096162-R-C22 project (Spanish Agencia Estatal de Investigación) for funding this research and for financial support of the contract of Enrique Sentandreu. Finally, authors are indebted to Igor Fochi (Thermo Fisher, Rodano, MI, Italy) for his technical support with CD3.2.

Appendix A. Supplementary data

Supplementary data to this article can be found online at https://doi.org/10.1016/j.foodchem.2022.135173.

References

Apaoblaza, A., Gerrard, S. D., Matarneh, S. K., Wicks, J. C., Kirkpatrick, L., England, E. M., … Gerrard, D. E. (2020). Muscle from grass- and grain-fed cattle differs energetically. *Meat Science, 161*, Article 107996. https://doi.org/10.1016/j.meatsci.2019.107996

Batchu, P., Terrill, T. H., Kouakou, B., Estrada-Reyes, Z. M., & Kannan, G. (2021). Plasma metabolomic profiles as affected by diet and stress in Spanish goats. *Scientific Reports, 11*(1), 12607. https://doi.org/10.1038/s41598-021-91893-x

Beauclercq, S., Nadal-Desbarats, L., Hennequet-Antier, C., Collin, A., Tesseraud, S., Bourin, M., … Berri, C. (2016). Serum and Muscle Metabolomics for the Prediction of Ultimate pH, a Key Factor for Chicken-Meat Quality. *Journal of Proteome Research, 15*(4), 1168–1178. https://doi.org/10.1021/acs.jproteome.5b01050

Benjamini, Y., & Hochberg, Y. (1995). Controlling the False Discovery Rate: A Practical and Powerful Approach to Multiple Testing. *Journal of the Royal Statistical Society: Series B (Methodological), 57*(1), 289–300. https://doi.org/10.1111/j.2517-6161.1995.tb02031.x

Breiman, L. (2001). Random Forests. *Machine Learning, 45*(1), 5–32. https://doi.org/10.1023/A:1010933404324

Cônsolo, N. R. B., Rosa, A. F., Barbosa, L. C. G. S., Maclean, P. H., Higuera-Padilla, A., Colnago, L. A., & Titto, E. A. L. (2021). Preliminary study on the characterization of Longissimus lumborum dark cutting meat in Angus × Nellore crossbreed cattle using NMR-based metabolomics. *Meat Science, 172*, Article 108350. https://doi.org/10.1016/j.meatsci.2020.108350

Dambrova, M., Zuurbier, C. J., Borutaite, V., Liepinsh, E., & Makrecka-Kuka, M. (2021). Energy substrate metabolism and mitochondrial oxidative stress in cardiac ischemia/reperfusion injury. *Free Radical Biology and Medicine, 165*, 24–37. https://doi.org/10.1016/j.freeradbiomed.2021.01.036

Dudzik, D., Barbas-Bernardos, C., García, A., & Barbas, C. (2018). Quality assurance procedures for mass spectrometry untargeted metabolomics. A review. *Journal of Pharmaceutical and Biomedical Analysis, 147*, 149–173. https://doi.org/10.1016/j.jpba.2017.07.044

Commission, E. (2004). Regulation (EC) N° 853/2004 of the European Parlament and of the Council of 29 April 2004 Laying down Specific Hygiene Rules for on the Hygiene of Foodstuffs. *Official Journal of the European Union, 139*(853), 55.

European Commission. COUNCIL REGULATION (EC) No 1099/2009 of 24 September 2009 on the Protection of Animals at the Time of Killing. Off. J. Eur. Union (2009) 1–30.

Fan, S., Kind, T., Cajka, T., Hazen, S. L., Tang, W. H. W., Kaddurah-Daouk, R., … Fiehn, O. (2019). Systematic error removal using random forest for normalizing large-scale untargeted lipidomics data. *Analytical Chemistry, 91*(5), 3590–3596. https://doi.org/10.1021/acs.analchem.8b05592

Ferguson, D. M., & Warner, R. D. (2008). Have we underestimated the impact of pre-slaughter stress on meat quality in ruminants? *Meat Science, 80*(1), 12–19. https://doi.org/10.1016/j.meatsci.2008.05.004

Fiems, L. O. (2012). Double muscling in cattle: Genes, husbandry carcasses and meat. *Animals, 2*(3), 472–506. https://doi.org/10.3390/ani2030472

Fuente-García, C., Aldai, N., Sentandreu, E., Oliván, M., Franco, D., García-Torres, S., & Sentandreu, M.Á. (2022). Assessment of caspase activity in post mortem muscle as a way to explain characteristics of DFD beef. *Journal of Food Composition and Analysis, 111*, Article 104599. https://doi.org/10.1016/j.jfca.2022.104599

Fuente-Garcia, C., Aldai, N., Sentandreu, E., Oliván, M., García-Torres, S., Franco, D., … Sentandreu, M. A. (2019). Search for proteomic biomarkers related to bovine pre-slaughter stress using liquid isoelectric focusing (OFFGEL) and mass spectrometry. *Journal of Proteomics, 198*, 59–65. https://doi.org/10.1016/j.jprot.2018.10.013

Fuente-Garcia, C., Sentandreu, E., Aldai, N., Oliván, M., & Sentandreu, M.Á. (2020). Characterization of the myofibrillar proteome as a way to better understand differences in bovine meats having different ultimate pH values. *Proteomics, 20*(12), 2000012. https://doi.org/10.1002/pmic.202000012

Fuente-García, C., Sentandreu, M. A., Aldai, N., Oliván, M., & Sentandreu, E. (2021). Proteomic pipeline for biomarker hunting of defective bovine meat assisted by liquid chromatography-mass spectrometry analysis and chemometrics. *Journal of Proteomics, 238*, Article 104153. https://doi.org/10.1016/j.jprot.2021.104153

Holdstock, J., Aalhus, J. L., Uttaro, B. A., López-Campos, Ó., Larsen, I. L., & Bruce, H. L. (2014). The impact of ultimate pH on muscle characteristics and sensory attributes of the longissimus thoracis within the dark cutting (Canada B4) beef carcass grade. *Meat Science, 98*(4), 842–849. https://doi.org/10.1016/j.meatsci.2014.07.029

Kasper, C., Ribeiro, D., de Almeida, A. M., Larzul, C., Liaubet, L., & Murani, E. (2020). Omics application in animal science—A special emphasis on stress response and damaging behaviour in pigs. *Genes, 11*(8), 920. https://doi.org/10.3390/genes11080920

Loudon, K. M. W., Lean, I. J., Pethick, D. W., Gardner, G. E., Grubb, L. J., Evans, A. C., & McGilchrist, P. (2018). On farm factors increasing dark cutting in pasture finished beef cattle. *Meat Science, 144*, 110–117. https://doi.org/10.1016/j.meatsci.2018.06.011

Makrecka, M., Kuka, J., Volska, K., Antone, U., Sevostjanovs, E., Cirule, H., … Liepinsh, E. (2014). Long-chain acylcarnitine content determines the pattern of energy metabolism in cardiac mitochondria. *Molecular and Cellular Biochemistry, 395*(1), 1–10. https://doi.org/10.1007/s11010-014-2106-3

Marco-Ramell, A., Gutiérrez, A. M., Velarde, A., Cerón, J. J., & Bassols, A. (2018). The Use of Proteomics to Study Biomarkers of Stress and Welfare in Farm Animals. In A. M. de Almeida, D. Eckersall, & I. Miller (Eds.), *Proteomics in Domestic Animals: From Farm to Systems Biology* (pp. 339–360). Springer International Publishing. https://doi.org/10.1007/978-3-319-69682-9_17.

McNeill, S. H., Harris, K. B., Field, T. G., & Van Elswyk, M. E. (2012). The evolution of lean beef: Identifying lean beef in today's U.S. marketplace. *Meat Science, 90*(1), 1–8. https://doi.org/10.1016/j.meatsci.2011.05.023

Muroya, S., Ueda, S., Komatsu, T., Miyakawa, T., & Ertbjerg, P. (2020). MEATabolomics: Muscle and meat metabolomics in domestic animals. *Metabolites, 10*(5), 188. https://doi.org/10.3390/metabo10050188

Nelson, D. L., & Cox, M. M. (2017). *Lehninger Principles of Biochemistry* (7th ed). Freeman Company: New York, W.H.

Ponnampalam, E. N., Hopkins, D. L., Bruce, H., Li, D., Baldi, G., & Bekhit, A. E. (2017). Causes and contributing factors to "Dark Cutting" Meat: Current trends and future directions: A review. *Comprehensive Reviews in Food Science and Food Safety, 16*(3), 400–430. https://doi.org/10.1111/1541-4337.12258

Righetti, L., Rubert, J., Galaverna, G., Hurkova, K., Dall'Asta, C., Hajslova, J., & Stranska-Zachariasova, M. (2018). A novel approach based on untargeted lipidomics reveals differences in the lipid pattern among durum and common wheat. Food Chemistry, 240, 775–783. 10.1016/j.foodchem.2017.08.020.

Schymanski, E. L., Jeon, J., Gulde, R., Fenner, K., Ruff, M., Singer, H. P., & Hollender, J. (2014). Identifying small molecules via high resolution mass spectrometry: Communicating confidence. *Environmental Science & Technology, 48*(4), 2097–2098. https://doi.org/10.1021/es5002105

Sentandreu, E., Fuente-García, C., Pardo, O., Oliván, M., León, N., Aldai, N., … Sentandreu, M. A. (2021). Protein biomarkers of bovine defective meats at a glance: Gel-free hybrid quadrupole-orbitrap analysis for rapid screening. *Journal of Agricultural and Food Chemistry, 69*(26), 7478–7487. https://doi.org/10.1021/acs.jafc.1c02016

Yusà, V., López, A., Dualde, P., Pardo, O., Fochi, I., Pineda, A., & Coscolla, C. (2020). Analysis of unknowns in recycled LDPE plastic by LC-Orbitrap Tribrid HRMS using MS3 with an intelligent data acquisition mode. *Microchemical Journal, 158*, Article 105256. https://doi.org/10.1016/j.microc.2020.105256